

# SUPERSONIC TURBULENT FUEL-AIR MIXING AND EVAPORATION

F. Moukalled<sup>1</sup> and M. Darwish<sup>2</sup>  
Mechanical Engineering Department,  
American University of Beirut,  
P.O.Box 11-0236  
Riad El Solh, Beirut 1107 2020  
Lebanon

Email: <sup>1</sup>[memouk@aub.edu.lb](mailto:memouk@aub.edu.lb), <sup>2</sup>[Darwish@aub.edu.lb](mailto:Darwish@aub.edu.lb)

## Abstract

Supersonic mixing and evaporation of poly-disperse sprays in complex flow systems are important in many engineering applications. The Eulerian and Lagrangian methods are two essentially different approaches for modeling such two-phase flows. Considering sprays consisting of droplets of various diameters, the Lagrangian approach accounts for each droplet discretely, while the Eulerian approach models the droplets, through an averaging process, as a continuum representing a second phase in addition to the gas phase. In this paper, adopting the Eulerian approach, an all speed control volume-based numerical procedure for predicting turbulent mixing and evaporation of droplets of variable diameters is formulated and implemented.

## Key words

evaporation, condensation, phase change, multi-phase flow.

## 1. Introduction

The design of modern gas turbines emphasizes high efficiency and low emissions to satisfy strict environmental legislations. To meet these requirements, new advanced combustion technology, such as Lean-Premix-Prevaporize (LPP) and Rich-Quench-Lean (RQL) is being introduced, and reliance on Computational Fluid Dynamics to accelerate the development process is increasing. Key aspects in this process are the models representing turbulent swirling flows, spray propagation and evaporation in addition to chemical reaction. Moreover, in supersonic combustors, the high flow velocities and short residence times require that fuel and air mix and burn quickly to avoid excessive long combustors. Therefore, understanding the nature of turbulent mixing and the need for means to augment the mixing process are essential in designing more efficient propulsive systems.

Approaches for the simulation of droplet transport and evaporation in combustors can be classified under two categories, namely the Lagrangian and Eulerian methods. In both methods the gaseous phase is calculated by solving the Navier-Stokes equations with a standard discretization method such as the Finite Volume Method.

The liquid phase however is treated differently in each approach.

In the framework of the **Lagrangian** method [1-5], the spray is represented by discrete droplets with each one characterizing a number of physical droplets that are observed and advected explicitly through the computational domain until it evaporates or exits through one of the boundaries. The equations of motion of the droplet in this case are a set of ordinary differential equations, which are solved by a numerical procedure different from that of the gaseous phase. To account for the interaction between the gaseous phase and the spray, several iterations of alternating solutions of the gaseous phase and the spray have to be conducted. Therefore, the computational effort for strongly interacting two-phase flows with the Lagrangian method is rather large. Furthermore, for turbulent flow simulation the above model has to be augmented with a stochastic or a Monte-Carlo approach.

In the **Eulerian** method [6-11], the evaporating spray is treated as an interacting and interpenetrating continuum, as such the resulting equations are similar to the equations describing the gaseous phase. This description allows the gaseous phase and the spray to be discretized by the same method, and therefore to be solved by the same numerical procedure. However, because of the presence of multiple phases, a multiphase algorithm needs to be used rather than a standard single-phase algorithm.

The model developed and implemented in this paper accounts for the heating and evaporation of multiple size droplets. The interaction of the gas and droplet phases is accounted for by using a two-phase multi-component Eulerian approach. The implementation is validated for subsonic and supersonic speeds and will form the basis for studying the more general problem of supersonic fuel mixing and combustion in the future.

In what follows the governing equations for droplet transport and evaporation are presented. Then, subsonic and supersonic turbulent evaporation results in a rectangular channel are discussed.

## 2. The governing equations

When describing multiphase flow phenomena it is implied that more than one phase exist within a small volume at any particular time. This view rests on the idea of time and space averaging [12,13] and is equivalent to

treating each phase as a continuum in the space under consideration, which requires choosing a proper scale with regard to the control volume used. For a multi-phase system the equations are derived over a representative element volume within which the different phases are present.

Except for the near region of the injector where the spray is dense, the volume fraction of the spray is low. In this dilute two-phase flow regime, interaction between droplets can be neglected. Starting from the Navier-Stokes equations, instantaneous transport equations for the gas and droplet phase can be derived either by spatial, temporal, or ensemble averaging. However, these transport equations can only be used for the description of sprays in laminar gas flows. Since combustors generally operate in the turbulent regime, the system of equations is extended by introducing turbulent fluctuations of the transport quantities followed by Reynolds averaging of the equations. For the gaseous phase, the standard  $k$ - $\varepsilon$  model is employed, while an algebraic model based on a Boussinesq approach approximates the turbulence terms in the droplet phase transport equations. The interacting flow fields are described by the transport equations presented next.

## 2.1 Gas equations

The continuity, momentum, energy, turbulence kinetic energy, and turbulence dissipation rate equations for the gas phase, which is composed of two species namely air and vapor, in addition to the mass fraction equation of the fuel vapor in the gaseous phase, are respectively written as:

$$\frac{\partial}{\partial t}(\alpha_g \rho_g) + \nabla \cdot (\alpha_g \rho_g \vec{v}_g) = \nabla \cdot \left( \frac{\mu_{t,g}}{Sc_{t,g}} \nabla \alpha_g \right) + I_{C,g} \quad (1)$$

$$\frac{\partial}{\partial t}(\alpha_g \rho_g \vec{v}_g) + \nabla \cdot (\alpha_g \rho_g \vec{v}_g \vec{v}_g) = -\alpha_g \nabla p + \nabla \cdot \vec{\tau}_g + \mathbf{F}_g^B + \mathbf{F}_g^D + I_{M,g} \quad (2)$$

$$\frac{\partial}{\partial t}(\alpha_g \rho_g k) + \nabla \cdot (\alpha_g \rho_g \vec{v}_g k) = \nabla \cdot \left( \alpha_g \frac{\mu_{eff,g}}{\sigma_k} \nabla k \right) + \alpha_g (P_k - \rho_g \varepsilon) + S_{k,d} \quad (3)$$

$$\frac{\partial}{\partial t}(\alpha_g \rho_g \varepsilon) + \nabla \cdot (\alpha_g \rho_g \vec{v}_g \varepsilon) = \nabla \cdot \left( \alpha_g \frac{\mu_{eff,g}}{\sigma_{T,\varepsilon}} \nabla \varepsilon \right) + \alpha_g \left( C_{\varepsilon 1} \frac{\varepsilon}{k} P_k - C_{\varepsilon 2} \rho_g \frac{\varepsilon^2}{k} \right) + S_{\varepsilon,d} \quad (4)$$

$$\frac{\partial}{\partial t}(\alpha_g \rho_g h_g) + \nabla \cdot (\alpha_g \rho_g \vec{v}_g h_g) = -\nabla \cdot \mathbf{q}_g + \nabla \cdot \left( \frac{\mu_{t,g}}{Pr_{t,g}} \nabla h_g \right) + I_{E,g} \quad (5)$$

$$\frac{\partial}{\partial t}(\alpha_g \rho_g Y_{vap,g}) + \nabla \cdot (\alpha_g \rho_g \vec{v}_g Y_{vap,g}) = \nabla \cdot (\alpha_g \Gamma_{Y_{vap,g}} \nabla Y_{vap,g}) + \mathbf{M}_{vap,g}^* (1 - Y_{vap,g}) \quad (6)$$

## 2.2 Droplet balance equations

Droplet evaporation is simulated by means of the Uniform Temperature model [2,4]. This computationally effective droplet model is based on the assumption of a homogeneous internal temperature distribution in the droplet and phase equilibrium conditions at the surface.

The analytical derivation of this model does not consider contributions to heat and mass transport through forced convection by the gas flow around the droplet. Forced convection is taken into account by means of two empirical correction factors ( $m_{correction}$  and  $h_{correction}$ ) [14].

$$\frac{\partial}{\partial t}(\alpha_d \rho_d) + \nabla \cdot (\alpha_d \rho_d \vec{v}_d) = \nabla \cdot \left( \frac{\mu_{t,d}}{Sc_{t,d}} \nabla \alpha_d \right) + I_{C,d} \quad (7)$$

$$\frac{\partial}{\partial t}(\alpha_d \rho_d \vec{v}_d) + \nabla \cdot (\alpha_d \rho_d \vec{v}_d \vec{v}_d) = -\alpha_d \nabla p + \nabla \cdot \vec{\tau}_d + \mathbf{F}_d^B + \mathbf{F}_d^D + I_{M,d} \quad (8)$$

$$\frac{\partial}{\partial t}(\alpha_d \rho_d h_d) + \nabla \cdot (\alpha_d \rho_d \vec{v}_d h_d) = \nabla \cdot \left( \frac{\mu_{t,d}}{Pr_{t,d}} \nabla h_d \right) + I_{E,d} \quad (9)$$

$$\frac{\partial}{\partial t}(\alpha_d \rho_d D) + \nabla \cdot (\alpha_d \vec{v}_d \rho_d D) = \nabla \cdot \left( \alpha_d \frac{\mu_{t,d}}{Pr_{t,d}} \nabla D \right) - \frac{8\alpha_d}{\pi D^2} \mathbf{M}_{vap}^* \quad (10)$$

where

$$I_{C,g} = -I_{C,g} = \frac{6\alpha_d}{\pi D^3} \mathbf{M}_{vap}^* \quad (11)$$

$$I_{M,g} = -I_{M,g} = \frac{6\alpha_d}{\pi D^3} \left( \frac{\pi}{8} D^2 \rho_g C_D |U_g - U_d| (U_g - U_d) + \mathbf{M}_{vap}^* U_d \right) \quad (12)$$

$$I_{E,g} = -I_{E,g} = \frac{6\alpha_d}{\pi D^3} (\mathbf{M}_{vap,s}^* + \mathbf{Q}_{cond,s}^*) \quad (13)$$

$$\mathbf{M}_{vap}^* = m_{correction} \mathbf{M}_{vap} \quad (14)$$

$$\mathbf{Q}_{cond,s}^* = \pi D^2 \alpha^* (T_d - T_g) \quad (15)$$

$$\mathbf{M}_{vap,s}^* = \mathbf{M}_{vap}^* c_{p,vap,ref} (T_d - T_g) \quad (16)$$

$$\mathbf{M}_{vap} = 2\pi D \rho_{g,ref} \Gamma_{im,ref} \ln \frac{1 - Y_{vap,g}}{1 - Y_{vap,s}} \quad (17)$$

$$\alpha^* = h_{correction} \frac{\frac{\mathbf{M}_{vap}^* c_{p,vap,ref}}{\pi D^2}}{\exp\left(\frac{\mathbf{M}_{vap}^* c_{p,vap,ref}}{2\pi D \lambda_{g,ref}}\right) - 1} \quad (18)$$

$$m_{correction} = 1 + 0.276 Re^{1/2} Sc^{1/3} \quad (19)$$

$$h_{correction} = 1 + 0.276 Re^{1/2} Pr^{1/3} \quad (20)$$

$$\mu_{turb,d} = \mu_{turb,g} \frac{\rho_d k_d}{\rho_g k_g} \quad (21)$$

For the two-phase flow considered, the volume fractions  $\alpha_g$  and  $\alpha_d$  are characterized by the condition:

$$\alpha_d + \alpha_g = 1 \quad (22)$$

The ratio of the turbulent kinetic energies of the dispersed and gas phase is calculated following the approach in [9,11]:

$$\frac{k_d}{k_g} = \frac{1}{1 + \omega^2 \tau^2} \quad (23)$$

where

$$k_d = \frac{1}{2} \vec{v}_d' \cdot \vec{v}_d' \quad (24)$$

Since in general the droplets do not follow the motion of the surrounding fluid from one point to another it is expected for the ratio  $k_d/k_g$  to be different from unity and varies with particle relaxation time  $t$  and local turbulence

quantities. Krämer [9] recommends the following equation for the frequency of the particle response:

$$\omega = \frac{1}{\tau} \left( \frac{\sqrt{\frac{2}{3}} k_g}{L_x} \tau \right)^{1/4} \quad (25)$$

$$\tau = \frac{1}{18} \frac{\rho_d}{\rho_g} \frac{D^2}{\nu} \frac{1}{1 + 0.133 \text{Re}_d^{0.687}}$$

with a characteristic macroscopic length scale of turbulence given by

$$L_x = (c_\mu)^{3/4} \frac{(k_g)^{3/2}}{\varepsilon_g} \quad (26)$$

### 3. Discretization procedure

A review of the above differential equations reveals that they are similar in structure. If a typical representative variable associated with phase (k) is denoted by  $\phi^{(k)}$ , the general fluidic differential equation may be written as:

$$\frac{\partial(\alpha^{(k)} \rho^{(k)} \phi^{(k)})}{\partial t} + \nabla \cdot (\alpha^{(k)} \rho^{(k)} \mathbf{u}^{(k)} \phi^{(k)}) = \nabla \cdot (\alpha^{(k)} \Gamma^{(k)} \nabla \phi^{(k)}) + \alpha^{(k)} Q^{(k)} \quad (27)$$

where the expression for  $\Gamma^{(k)}$  and  $Q^{(k)}$  can be deduced from the parent equations.

The general conservation equation (27) is integrated over a finite volume to yield:

$$\iint_{\Omega} \frac{\partial(\alpha^{(k)} \rho^{(k)} \phi^{(k)})}{\partial t} d\Omega + \iint_{\Omega} \nabla \cdot (\alpha^{(k)} \rho^{(k)} \mathbf{u}^{(k)} \phi^{(k)}) d\Omega = \iint_{\Omega} \nabla \cdot (\alpha^{(k)} \Gamma^{(k)} \nabla \phi^{(k)}) d\Omega + \iint_{\Omega} \alpha^{(k)} Q^{(k)} d\Omega \quad (28)$$

Where  $\Omega$  is the volume of the control cell. Using the divergence theorem to transform the volume integral into a surface integral, replacing the surface integrals by a summation of the fluxes over the sides of the control volume, and then discretizing these fluxes using suitable interpolation profiles (the High Resolution SMART [15] scheme is employed and applied within the context of the NVSF methodology [16]) the following algebraic equation results:

$$A_P^{(k)} \phi_P^{(k)} = \sum_{NB} A_{NB}^{(k)} \phi_{NB}^{(k)} + B_P^{(k)} \quad (29)$$

In compact form, the above equation can be written as

$$\phi^{(k)} = H_P \left[ \phi^{(k)} \right] = \frac{\sum_{NB} A_{NB}^{(k)} \phi_{NB}^{(k)} + B_P^{(k)}}{A_P^{(k)}} \quad (30)$$

An equation similar to equation (29) is obtained at each grid point in the domain and the collection of these equations forms a system that is solved iteratively.

The discretization procedure for the momentum equation yields an algebraic equation of the form:

$$\mathbf{u}_P^{(k)} = \mathbf{H} \mathbf{P}_P \left[ \mathbf{u}^{(k)} \right] - \alpha^{(k)} \mathbf{D}_P^{(k)} \nabla_P (P) \quad (31)$$

Furthermore, the phasic mass-conservation equation can be viewed as a phasic volume fraction equation, which can be written as:

$$\alpha_P^{(k)} = H_P \left[ \alpha^{(k)} \right] \quad (32)$$

or as a phasic continuity equation to be used in deriving the pressure correction equation:

$$\frac{(\alpha_P^{(k)} \rho_P^{(k)}) - (\alpha_P^{(k)} \rho_P^{(k)})^{\text{Old}}}{\partial t} \Omega + \Delta_P \left[ \alpha^{(k)} \rho^{(k)} \mathbf{u}^{(k)} \cdot \mathbf{S} \right] = \alpha^{(k)} \mathbf{M}^{(k)} \quad (33)$$

where the  $\Delta$  operator represents the following operation:

$$\Delta_P [\Theta] = \sum_{f=nb(P)} \Theta_f \quad (34)$$

#### 3.1 Pressure correction equation

To derive the pressure-correction equation, the mass conservation equations of the various fluids are added to yield the global mass conservation equation given by:

$$\sum_k \left\{ \frac{(\alpha_P^{(k)} \rho_P^{(k)}) - (\alpha_P^{(k)} \rho_P^{(k)})^{\text{Old}}}{\partial t} \Omega + \Delta_P (\alpha^{(k)} \rho^{(k)} \mathbf{u}^{(k)} \cdot \mathbf{S}) \right\} = 0 \quad (35)$$

Denoting the corrections for pressure, density, and velocity by  $P'$ ,  $\mathbf{u}^{(k)'}$ , and  $\rho^{(k)'}$ , respectively, the corrected fields are written as:

$$P = P^o + P', \mathbf{u}^{(k)} = \mathbf{u}^{(k)o} + \mathbf{u}^{(k)'}, \rho^{(k)} = \rho^{(k)o} + \rho^{(k)'} \quad (36)$$

Combining equations (31), (35), and (36), the final form of the pressure-correction equation is obtained as [17]:

$$\sum_k \left\{ \frac{\Omega}{\partial t} r_P^{(k)o} C_\rho^{(k)} P' + \Delta_P \left[ r^{(k)o} U^{(k)*} C_\rho^{(k)} P' \right] - \Delta_P \left[ r^{(k)o} \rho^{(k)*} \left( r^{(k)o} \mathbf{D}^{(k)} \nabla P' \right) \cdot \mathbf{S} \right] \right\} = - \sum_k \left\{ \frac{r_P^{(k)o} \rho_P^{(k)*} - (r_P^{(k)} \rho_P^{(k)})^{\text{old}}}{\partial t} \Omega + \Delta_P \left[ r^{(k)o} \rho^{(k)*} U^{(k)*} \right] \right\} \quad (37)$$

The corrections are then applied to the velocity, density, and pressure fields using the following equations:

$$\mathbf{u}_P^{(k)*} = \mathbf{u}_P^{(k)o} - r^{(k)o} \mathbf{D}_P^{(k)} \nabla_P P', \quad P^* = P^o + P', \rho^{(k)*} = \rho^{(k)o} + C_\rho^{(k)} P' \quad (38)$$

#### 3.2 MCBA-SIMPLE Algorithm

The overall solution procedure is an extension of the single-phase SIMPLE algorithm into multi-phase flows. Since the pressure correction equation is derived from overall mass conservation, it is denoted by MCBA-SIMPLE [17]. The sequence of events in the MCBA-SIMPLE is as follows:

- Solve the fluidic momentum equations for velocities.
- Solve the pressure correction equation based on global mass conservation.
- Correct velocities, densities, and pressure.
- Solve the fluidic mass conservation equations for volume fractions.
- Solve the fluidic scalar equations (k,  $\varepsilon$ , T, Y, D, etc...).
- Return to the first step and repeat until convergence.

## 4. Results and discussion

The above described method has been implemented within a finite volume code and used to generate solutions for laminar, turbulent, subsonic, and supersonic evaporation and mixing of water droplets in air. For that purpose, preliminary results for three two-dimensional two-phase flow problems are presented. The physical situation for these problems, depicted in Fig. 1, represents a rectangular duct in which air enters with a uniform free stream velocity  $U$ , while fuel (water is used here) mixed with air is injected along a central portion of width  $d$  ( $d=3W/21$ ). The length of the domain is  $L$  ( $L=1$  m) and its width is  $W$  ( $W=0.25$  m). In all problems, the domain is subdivided into  $42 \times 23$  uniform control volumes, the fuel is injected through 3 control volumes with velocities that are equal in magnitude ( $=20\%$  of the free stream velocity) but with different injection angles (making  $-45^\circ$ ,  $0^\circ$ , and  $45^\circ$  with the horizontal as shown in Fig. 1). Moreover, the required temperature dependent properties of the carrier gas (air) and vapor species are given by [18]:

For air

$$\begin{aligned} MW_{\text{air}} &= 28.97 \text{ kg / kg mole} \\ \mu_{\text{air}} &= 6.109 \times 10^{-6} + 4.604 \times 10^{-8} T - 1.051 \times 10^{-11} T^2 \text{ Kg / m.s} \\ \lambda_{\text{air}} &= 3.227 \times 10^{-3} + 8.3894 \times 10^{-5} T - 1.9858 \times 10^{-8} T^2 \text{ J / m.s.K} \\ Pr_{\text{air}} &= 0.815 - 4.958 \times 10^{-4} T + 4.514 \times 10^{-7} T^2 \text{ for } T \leq 600 \text{ K} \\ Pr_{\text{air}} &= 0.647 + 5.5 \times 10^{-5} T \text{ for } T > 600 \text{ K} \end{aligned} \quad (39)$$

For water and water vapor

$$\begin{aligned} MW_{\text{water}} &= 18.015 \text{ kg / kg mole} \\ c_{p,v} &= 8137 - 37.34 \times T + 0.07482 \times T^2 - 4.956 \times 10^{-5} T^3 \text{ J / kg.K} \\ \mu_v &= 4.07 \times 10^{-8} T - 3.077 \times 10^{-6} \text{ Kg / m.s} \\ \lambda_v &= 1.024 \times 10^{-2} - 8.21 \times 10^{-6} T + 1.41 \times 10^{-7} T^2 - 4.51 \times 10^{-11} T^3 \text{ J / m.s.K} \\ L_v &= 2.257 \times 10^6 + 2.595 \times 10^3 (373.15 - T) \text{ J / kg} \\ \rho_L &= 997 \text{ kg / m}^3 \quad c_L = 4184 \text{ J / kg.K} \quad \lambda_L = 0.6531 \text{ J / m.s.K} \end{aligned} \quad (40)$$

It is further assumed that the Lewis number is equal to unity and the diffusivity ( $\Gamma$ ) is calculated with the density evaluated at the reference temperature.

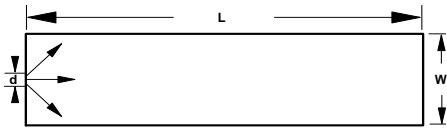


Fig. 1 Physical domain.

### 4.1 Subsonic laminar evaporation and mixing

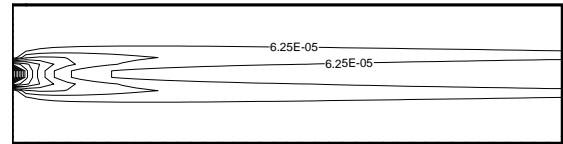
In this problem the Mach number and temperature of the air at inlet to the domain are taken to be 0.1 ( $M_{\text{air,inlet}}=0.1$ ) and 900 K, respectively. The mixture of air and droplet enters the domain at a temperature of 300 K with the volume fraction of the water in the injected air-water mixture being  $10^{-3}$ . Results generated are depicted in Figs. 2 and 3. In Fig. 2(a) the droplet volume fraction and velocity fields are depicted. As shown, due to the higher air velocity, the spreading of injected water is low and droplets quickly align with the air velocity. As expected, the gas temperature (Fig. 2(b)) is minimized along the

centerline of the domain. This decrease in temperature is associated with an increase in density (Fig. 2(c)). The distribution of the water vapor in the gas phase is displayed in Fig. 2(d). The mass fraction of the water vapor in the gas phase increases as the mixture moves downstream in the channel due to the increase in the evaporated amount with distance, which is physically plausible. Computations have shown that 32.4% of the water droplets entering the domain are transformed into water vapor.

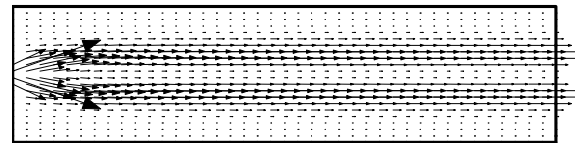
The decrease in the droplet diameter along the centerline of the channel is depicted in Fig. 3(a), while the increase in the droplet temperature there is displayed in Fig. 3(b). The rate of increase is high in the early part of the channel where 90% of the total increase occurs over almost 15% of the channel length due to the relatively low gas velocity. This decrease in temperature is associated with a decrease in the rate of evaporation, which explains the slight increase in the rate at which the diameter decreases.

### 4.2 Subsonic turbulent evaporation and mixing

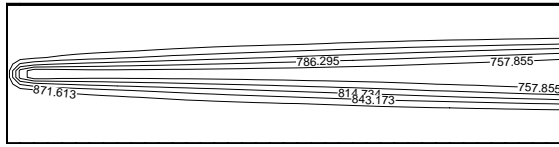
For the same input as in problem 1, the Mach number is increased to 0.4, the k- $\epsilon$  model is invoked and results for turbulent conditions are generated. Results are depicted in Figs. 4 and 5. Due to turbulence and the larger velocities involved, higher mixing is obtained (Figs. 4(a)-4(d)). The drop in temperature is less than in the previous cases (Fig. 4(b)) however it occurs over a wider area of the domain. Similar spreading is seen for the gas density (Fig. 4(c)) and the water vapor mass fraction (Fig. 4(d)). Due to the higher velocity and consequently shorter residence time of the mixture in the channel, only 12.4% of the water droplets entering the domain are transformed into water vapor in comparison to 32.78% for the  $M_{\text{air,inlet}}=0.1$  case. This lower evaporation rate is reflected by the small decrease in the droplet diameter, in comparison with the previous case, depicted in Fig. 5(a). Moreover, the rate of increase in the droplet temperature is lower than in the previous case (Fig. 5(b)). Again this is caused by the higher velocities, which allows less time for heat transfer between the droplets and gas.



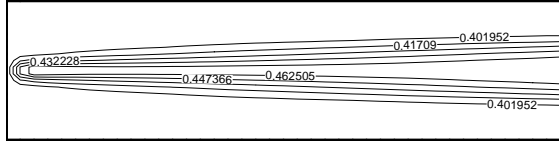
(a)



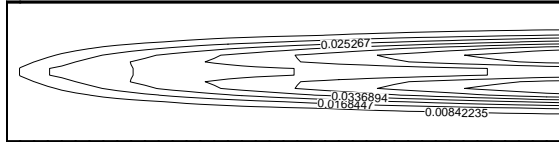
(b)



(c)

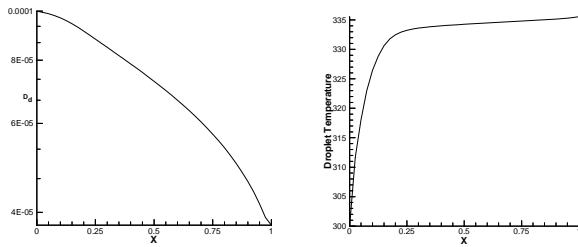


(d)



(e)

Fig. 2 (a) droplet volume fraction, (b) velocity field, (c) gas temperature, (d) gas density, and (e) mass fraction of water vapor ( $M=0.1$ , laminar).



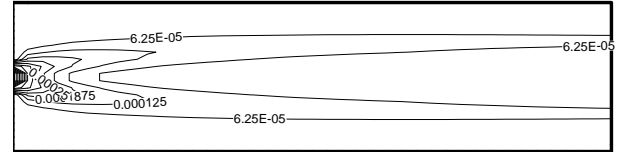
(a) (b)

Fig. 3 (a) Variation of droplet diameter and (b) droplet temperature along the center line of the domain.

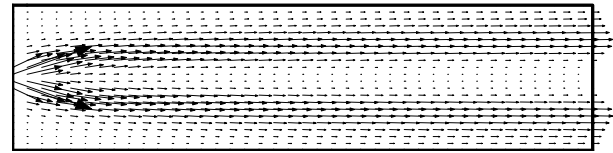
### 4.3 Supersonic turbulent evaporation and mixing of water droplets in air

For the same physical situation depicted in Fig. 1, the Mach number of the air at inlet to the domain is set to 2 ( $M_{air,inlet}=2$ ). All other parameters are similar to those used earlier. Turbulent flow results for this case are presented in Figs. 6 and 7. Due to the higher velocity, deeper penetration of the water droplet is accomplished (Fig. 6(a)). The gas temperature decreases along the centerline of the domain and increases close to the walls (Fig. 6(b)) due to the use of a Neumann boundary condition, which causes heat generated by viscous dissipation to be trapped in the boundary layer region. Moreover, the gas density (Fig. 6(c)) is higher in regions where the water vapor mass fraction is higher (Fig. 6(d)) and both increase as the mixture moves downstream in the channel due to the increase in the evaporated amount with distance. Computations have shown that only 3.41% of the water droplets entering the domain are transformed into water vapor due to the high velocities involved and consequently short residence time of water droplets. The decrease in the droplet diameter along the centerline of the channel is depicted in Fig. 7(a), while the increase

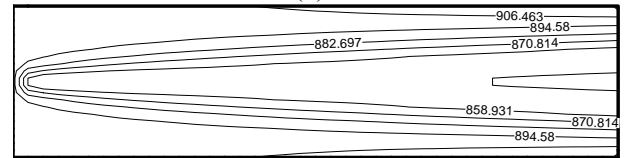
in the droplet temperature there is displayed in Fig. 7(b). Lower decrease in the droplet diameter is obtained as compared to the previous cases, which is in line with the lower evaporation rate. Moreover, the rate of increase in temperature is still higher in the early part of the channel but it occurs at a much lower rate than the previous subsonic cases and is spread over most of the channel length.



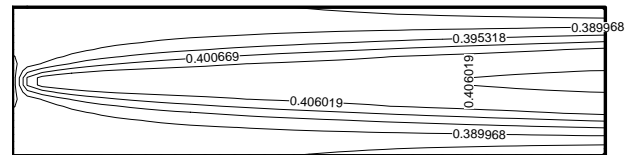
(a)



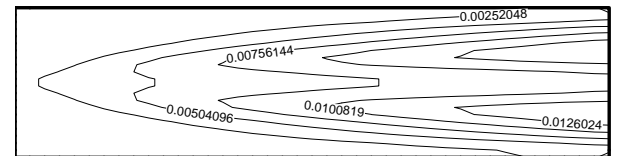
(b)



(c)

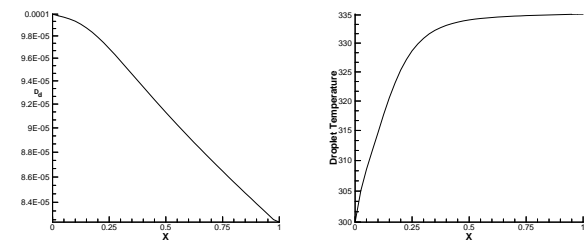


(d)



(e)

Fig. 4 (a) droplet volume fraction, (b) velocity field, (c) gas temperature, (d) gas density, and (e) mass fraction of water vapor ( $M=0.4$ , turbulent).



(a) (b)

Fig. 5 (a) Variation of droplet diameter and (b) droplet temperature along the center line of the domain.

## 5. Conclusion

An Eulerian model for the prediction of variable size droplet evaporation and mixing at all speeds was

presented. The model was tested by solving evaporation and mixing problems in the various Mach number regimes. Results obtained are promising but still need validation against published data. Even though water was used for the droplets, this is not a model restriction and multi-component fuels can be equally used as droplet materials. Also a number of numerical issues are currently being addressed. These and a fuel-air system implementation will be our next step focus.

## 6. Acknowledgement

The financial support provided by the University Research Board of the American University of Beirut is gratefully acknowledged.

## REFERENCES

- [1] Abramzon, B. and Sirignano, W.A., "Droplet Vaporization Models for spray Combustion calculations," *International Journal of Heat and Mass Transfer*, vol. 32, pp. 1605-1618, 1989.
- [2] Aggarwal, S.K. and Peng, F., "A review of Droplet Dynamics and Vaporization Modeling for Engineering Calculations," *ASME Journal of Engineering for Gas Turbine and Power*, vol. 117, pp. 453-461, 1995.
- [3] Crowe, C.T., Sharma, M.P., and Stock, D.E., "The Particle-Source-In Cell (PSI-CELL) Model for Gas-Droplet Flows," *ASME Journal of Fluids Engineering*, vol. 99, pp. 325-332, 1977.
- [4] Faeth, G.M., "Evaporation and Combustion of Sprays," *Prog. Energy Combust. Sci.*, vol. 9, pp. 1-76, 1983.
- [5] Mostafa, A.A. and Mongia, H.C., "On the Modeling of Turbulent Evaporating Sprays: Eulerian versus Lagrangian Approach," *International Journal of Heat and Mass Transfer*, vol. 30, no. 12, pp. 2583-2593, 1987.
- [6] Mellville, W.K. and Bray, K.N.C., "A Model of the Two-Phase Turbulent Jet," *International Journal of Heat and Mass Transfer*, vol. 22, pp. 647-656, 1979.
- [7] Elgobashi, S.E., Abou-Arab, T.W., Rizk, M., and Mostafa, A., "Prediction of the Particle-Laden Jet with a Two-Equation Turbulence Model," *International Journal of Multiphase flow*, vol. 10, no. 6, pp. 697-710, 1984.
- [8] Chen, C.P. and Wood, P.E., "Turbulence Closure Modeling of the Dilute Gas-Particle Axisymmetric Jet," *AIChE-Journal*, vol. 32, no. 1, pp. 163-166, 1986.
- [9] Krämer, M., "Untersuchungen zum Bewegungsverhalten von Tropfen in turbulenter Strömung im Hinblick auf Verbrennungsvorgänge" Dissertation, Institut für Feuerungstechnik, Universität Karlsruhe (T.H.), 1988.
- [10] Abou-Arab, T.W. and Roco, M.C., "Solid Phase Contribution in the Two-Phase Turbulent Kinetic Energy Equation," *ASME Journal of Fluids Engineering*, vol. 112, pp. 351-361, 1990.
- [11] Wittig S., Hallmann M., Scheirlen M., Schmehl R., "A new Eulerian model for turbulent evaporating sprays in recirculating flows", AGARD Meeting on "Fuel Combustion Technology for advanced Aircraft Engines, May 1993.
- [12] Hassanizadeh M., Gray W.G. "General Conservation Equations for multi-phase systems, I Averaging procedure", *Adv. Water Resources*, vol. 2, pp. 131-190, 1979.
- [13] Hassanizadeh M., Gray W.G., "General Conservation Equations for Multi-Phase Systems: 2, Mass, Momenta, Energy and Entropy Equations", *Adv. Water Res.*, vol. 2, pp. 191-202, 1979.
- [14] Frössling, N., "Über die Verdunstung fallender Tropfen," *Gerlands Beiträge zur Geophysik*, vol. 52, pp. 170-215, 1938.
- [15] Gaskell, P.H. and Lau, A.K.C., Curvature Compensated Convective Transport: SMART, A New Boundedness Preserving Transport Algorithm, *Int. J. Num. Meth. Fluids*, 8, pp. 617-641, 1988.

[16] Darwish, M.S. and Moukalled, F., Normalized Variable and Space Formulation Methodology For High-Resolution Schemes, *Numerical Heat Transfer, Part B*, vol. 26, pp. 79-96, 1994.

[17] Darwish, M., Moukalled, F., and, Sekar, B., A Unified Formulation of the Segregated Class of Algorithms for Multi-phase Flow at All Speeds, *Numerical Heat Transfer, Part B*, 40(2), pp. 99-137, 2001.

[18] Harpole, G.M., "Droplet Evaporation in High Temperature Environment," *Journal of Heat Transfer*, vol. 103, pp. 86-91, 1981.

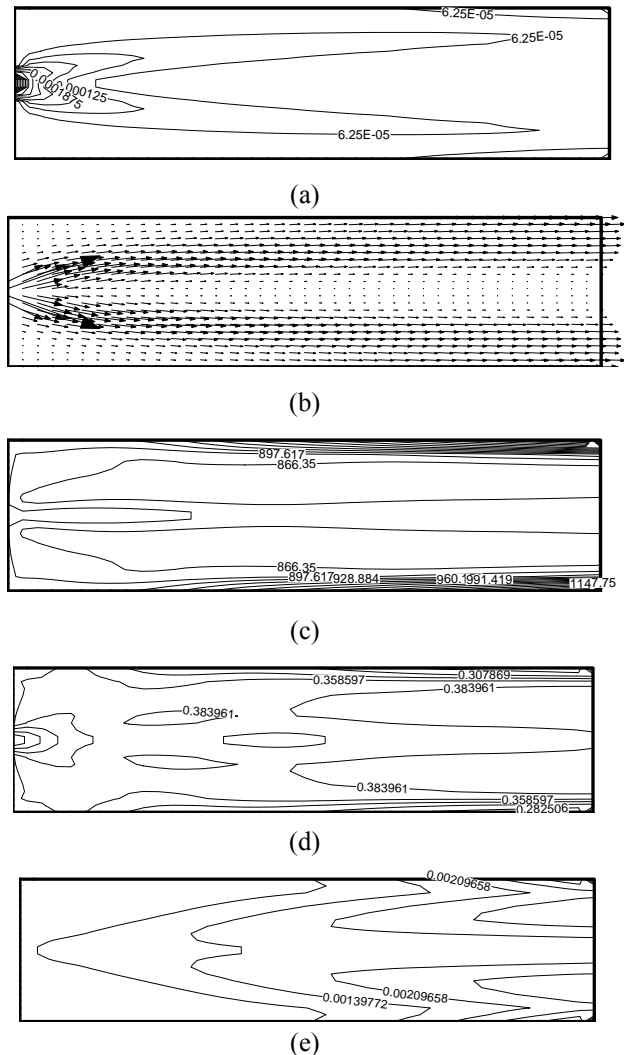


Fig. 6 (a) droplet volume fraction, (b) velocity field, (c) gas temperature, (d) gas density, and (e) mass fraction of water vapor (supersonic  $M=2$ , turbulent).

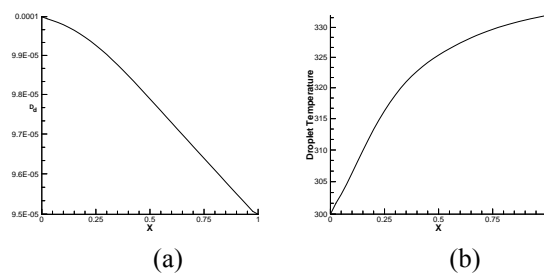


Fig. 7 (a) Variation of droplet diameter and (b) droplet temperature along the center line of the domain.